Analog Integrated Circuits and Signal Processing, 19, 223–239 (1999)

Design of High Dynamic Range Fully Integratable Translinear Filters

WOUTER A. SERDIJN, MICHIEL H. L. KOUWENHOVEN, JAN MULDER AND ARTHUR H. M. VAN ROERMUND

Delft University of Technology, Faculty of Electrical Engineering/DIMES Mekelweg 4, 2628 CD Delft, The Netherlands, E-mail: W.A.Serdijn@et.tudelft.nl

Received November 7, 1996; Revised July 21, 1997; Accepted December 17, 1997

Abstract. This paper addresses the non-linear noise and dynamic-range properties of bipolar and MOS (both in weak and in strong inversion) translinear integrators, following a systematic top-down approach. Several design principles to achieve an optimal dynamic range are derived. A qualitative comparison of a bipolar or weak-inversion class-AB translinear integrator and the well-known linear $g_m - C$ integrator reveals that the former is an interesting candidate, especially for low-voltage and/or low-power operation. As an example, a $\pm$ 1.65-V bipolar translinear integrator is presented that makes dynamic-range optimization possible by adjusting just one bias current. Its application in an audio filter yields a 63-dB dynamic range and a virtual dynamic range of 76 dB, while the current consumption can be as low as 310 nA.

Key Words: non-linear noise, dynamic range, translinear, dynamic translinear, log-domain, integrator, filters

1. Introduction

Recently, both a current-mode analysis method and a synthesis method for dynamic translinear circuits were proposed by the authors [1–3]. The dynamic translinear principle can be regarded as a generalization of the well-known ''static'' translinear principle, formulated by Gilbert in 1975 [4].

An important subclass of dynamic translinear circuits is the class of ''translinear filters'', also called ''log-domain'' or ''exponential state-space'' filters, which were originally introduced by Adams in 1979 [5]. Although not recognized then, this was actually the first time a first-order linear differential equation was implemented using translinear circuit techniques. In 1990, Seevinck introduced a ''companding current-mode integrator'' [6] and since then the principle of translinear filtering has been extensively studied by Frey, see, e.g. [7], Punzenberger and Enz, see e.g. [8], Toumazou et al. see, e.g. [9], Roberts et al. [10], Tsividis, see, e.g. [11] and Mulder and Serdijn, see e.g. [12,13].

Using the dynamic translinear principle, it is possible to implement almost every linear or non-linear differential equation, using transistors and capacitors only. See, e.g. [14,15]. Hence, a high functional density can be obtained, whereas the absence of large resistors makes them especially interesting for ultra-low-power applications [16].

Apart from this, dynamic translinear circuits also exhibit other interesting properties.

1. Owing to the exponential behavior of a bipolar transistor or a MOS transistor in its subthreshold region, the voltages in dynamic translinear circuits are logarithmically related to the currents. As a result, the voltage excursions are small, typically only a few tens of millivolts. This is beneficial in a low-voltage environment.
2. Due to these small voltage swings, the effects of parasitic capacitances are reduced. This facilitates relatively wide bandwidth operation [17,18].
3. Dynamic translinear circuits are easily controlled over a wide range of several parameters, such as gain, frequency or threshold. This increases their designability and makes them attractive to be implemented as standard cells or programmable building blocks.
4. In dynamic translinear circuits, transistors are used either as elements of the translinear loops or as nullors, to provide additional loop gain or to

counteract the transistor second-order effects. Hence, in an IC process only three types of components are required:

- transistors that are well matched and have an accurate exponential transfer over a wide range of transistor current,
- transistors with a large gain, also at higher frequencies, and
- capacitors.

In this paper, the dynamic range properties of translinear integrators, which can be considered to be a basic building block of translinear filters, are investigated at function level. Section 2 highlights the key idea behind companding integrators, of which translinear integrators form an important subclass. In Section 3, the effect of possible noise sources on the output noise is analyzed and several design principles for optimal-dynamic-range translinear integrators are formulated. As an example, in Section 4, a $\pm$ 1.65-V bipolar translinear integrator is presented that makes dynamic range optimization possible by adjusting just one bias current.

2. Companding Integrators

As a starting point, let us consider the block diagram of a companding integrator, as mentioned by Seevinck [6], comprising a divider, a linear time integrator, an expander block F that generates the output signal y from some internal quantity v, $y = F(v)$, and a block F' that generates the derivative of the output signal y with respect to v. See Fig. 1. This integrator can be considered to be an implementation of a first-order linear differential equation $x(t) = dy(t)/dt$ by applying the chain rule:

$$x(t) = \frac{dy(t)}{dt} = \frac{dy(t)}{dv(t)} \cdot \frac{dv(t)}{dt} = \frac{dF[v(t)]}{dv(t)} \cdot \frac{dv(t)}{dt} \qquad (1)$$

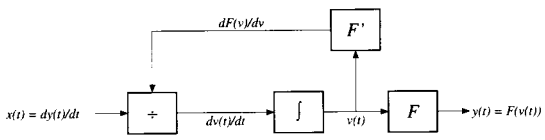

Fig. 1. General block diagram of a companding integrator.

Note that this differential equation is completely independent of $v(t)$. Moreover, if F is an expanding function, the variation of v for a given variation of x will be less than for a linear F.

Hence, with regard to the overall transfer function, the only demands made on F and F' are that both functions are integratable and that F is expanding. Therefore, the exact implementations of F and F' must be based on other important design aspects, such as dynamic range, bandwidth and power efficiency, all being major design aspects in a low-voltage low-power environment.

3. Dynamic Range

To gain insight into the dynamic range of this companding integrator, several additive uncorrelated, possibly non-stationary, noise sources from real Gaussian random processes with zero mean, i.e. having a flat spectral density, are assumed to be present, as indicated in Fig. 2.

In the presence of these noise sources, the output signal of the companding integrator becomes

$$y = F(v) + \varepsilon_4 \qquad (2)$$

Its time derivative, applying the chain-rule, becomes

$$\frac{dy}{dt} = \frac{d\varepsilon_4}{dt} + \frac{dF(v)}{dv} \cdot \frac{dv}{dt} \qquad (3)$$

Since

$$\frac{dF(v)}{dv} = y' - \varepsilon_3 \text{ and} \qquad (4)$$

$$\frac{dv}{dt} = \varepsilon_2 + \frac{x + \varepsilon_1}{y'} \qquad (5)$$

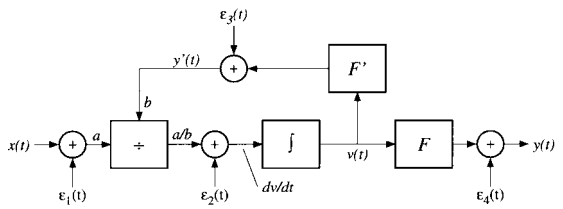

Fig. 2. The companding integrator including its (additive) noise sources.

it follows that

$$\frac{dy}{dt} = \frac{d\varepsilon_4}{dt} + (y' - \varepsilon_3)\left(\frac{x+\varepsilon_1}{y'} + \varepsilon_2\right) \tag{6}$$

$$= x + \varepsilon_1 + \varepsilon_2 \cdot y' - \varepsilon_3 \cdot \frac{x}{y'} + \frac{d\varepsilon_4}{dt} - \frac{\varepsilon_1\varepsilon_3}{y'} - \varepsilon_2\varepsilon_3 \tag{7}$$

Note that ε_1 and ε_4 are simply added to x and y, respectively, which is obvious since ε_1 and ε_4 are situated directly at the input and output of the integrator, respectively.

If the noise × noise terms and the signal × noise terms of second and higher order in $\varepsilon_n (n \in [1,4])$ are considered to be of minor importance, the latter two terms in (7) can be neglected and the term y' may be considered to be noise-free.

Using

$$\begin{aligned} y' = F'(v) &= \frac{dF}{dv}(v) = \frac{dF}{dv}[F^{-1}(y)] \\ &= \frac{dF}{dv}\left[F^{-1}\left(\int^t x(\tau)d\tau\right)\right] \end{aligned} \tag{8}$$

it follows that

$$\frac{dy}{dt} = x + \varepsilon_1 + \varepsilon_2 \cdot G_1(x,t) - \varepsilon_3 \cdot G_2(x,t) + \frac{d\varepsilon_4}{dt} \tag{9}$$

with

$$G_1(x,t) = \frac{dF}{dv}\left[F^{-1}\left(\int^t x(\tau)d\tau\right)\right] \text{ and} \tag{10}$$

$$G_2(x,t) = \frac{x(t)}{\frac{dF}{dv}\left[F^{-1}\left(\int^t x(\tau)d\tau\right)\right]} = \frac{x(t)}{G_1(x,t)} \tag{11}$$

Assuming $x, \varepsilon_1, \varepsilon_2, \varepsilon_3$ and ε_4 to be uncorrelated, the autocorrelation function of dy/dt becomes

$$\begin{aligned} R_{dy/dt}(t,\tau) &= R_x(t,\tau) \\ &\quad + R_{\varepsilon_1}(t,\tau) \\ &\quad + E_{\varepsilon_2,x}\{\varepsilon_2(t) \cdot G_1[x(t),t] \cdot \varepsilon_2(t+\tau) \\ &\qquad \cdot G_1[x(t+\tau),t+\tau]\} \\ &\quad + E_{\varepsilon_3,x}[\varepsilon_3(t) \cdot G_2(x(t),t) \cdot \varepsilon_3(t+\tau) \\ &\qquad \cdot G_2(x(t+\tau),t+\tau)] \\ &\quad + R_{d\varepsilon_4/dt}(\tau) \end{aligned} \tag{12}$$

$$\begin{aligned} &= R_x(t,\tau) \\ &\quad + R_{\varepsilon_1}(t,\tau) \\ &\quad + E_{\varepsilon_2}[\varepsilon_2(t) \cdot \varepsilon_2(t+\tau)] \cdot E_x\{G_1[x(t),t] \\ &\qquad \cdot G_1[x(t+\tau),t+\tau]\} \\ &\quad + E_{\varepsilon_3}[\varepsilon_3(t) \cdot \varepsilon_3(t+\tau)] \cdot E_x\{G_2[x(t),t] \\ &\qquad \cdot G_2[x(t+\tau),t+\tau]\} \\ &\quad + R_{d\varepsilon_4/dt}(\tau) \end{aligned} \tag{13}$$

$$\begin{aligned} &= R_x(t,\tau) \\ &\quad + R_{\varepsilon_1}(t,\tau) \\ &\quad + R_{\varepsilon_2}(t,\tau) \cdot R_{G_1}(t,\tau) \\ &\quad + R_{\varepsilon_3}(t,\tau) \cdot R_{G_2}(t,\tau) \\ &\quad + R_{d\varepsilon_4/dt}(\tau) \end{aligned} \tag{14}$$

$E[(\cdot)]$ being the mathematical expectation of $(\cdot)$.

According to the Wiener-Khintchine theorem for non-stationary processes [19], a power density spectrum of dy/dt can be calculated from the autocorrelation function of dy/dt, which yields:

$$\begin{aligned} S_{dy/dt}(\omega,t) &= S_x(\omega,t) + S_{\varepsilon_1}(\omega,t) \\ &\quad + S_{\varepsilon_2}(\omega,t) * S_{G_1}(\omega,t) \\ &\quad + S_{\varepsilon_3}(\omega,t) * S_{G_2}(\omega,t) \\ &\quad + S_{d\varepsilon_4/dt}(\omega,t) \end{aligned} \tag{15}$$

Assuming $\varepsilon_n (n \in [1,4])$ to have a white spectrum, which is true for the thermal noise generated by a MOS transistor in strong inversion and for the shot noise of a bipolar or weak-inversion MOS transistor, $S_{\varepsilon_n}(\omega,t) = S_{\varepsilon_n}(t)$ are functions of time only and the above expression for $S_{dy/dt}(\omega,t)$ simplifies to

$$\begin{aligned} S_{dy/dt}(\omega,t) &= S_x(\omega,t) \\ &\quad + S_{\varepsilon_1}(t) + \frac{S_{\varepsilon_2}(t)}{2\pi}\int_0^\infty S_{G_1}(z,t)dz \\ &\quad + \frac{S_{\varepsilon_3}(t)}{2\pi}\int_0^\infty S_{G_2}(z,t)dz \\ &\quad + S_{d\varepsilon_4/dt}(\omega,t) \end{aligned} \tag{16}$$

$$= S_x(\omega,t) + S_{\varepsilon_1}(t) + S_{\varepsilon_2}(t)\cdot E_x[G_1^2(x,t)] + S_{\varepsilon_3}(t)\cdot E_x[G_2^2(x,t)] + S_{d\varepsilon_4/dt}(\omega,t) \quad (17)$$

Since

$$y = \int \frac{dy}{dt}dt \text{ and thus} \quad (18)$$

$$S_y(\omega,t) = S_{dy/dt}(\omega,t)\cdot\frac{1}{\omega^2} \quad (19)$$

we finally end up with

$$S_y(\omega,t) = S_x(\omega,t)\cdot\frac{1}{\omega^2} + S_{\varepsilon_1}(t)\cdot\frac{1}{\omega^2} + S_{\varepsilon_2}(t)\cdot\frac{E_x[G_1^2(x,t)]}{\omega^2} + S_{\varepsilon_3}(t)\cdot\frac{E_x[G_2^2(x,t)]}{\omega^2} + S_{\varepsilon_4}(t) \quad (20)$$

Assuming that the (single-sided) bandwidth of interest ranges from ω_1 to ω_2, it follows that the total (instantaneous) signal power at the output of the integrator equals

$$P_S(t) = \frac{1}{2\pi}\int_{\omega_1}^{\omega_2} S_x(\omega,t)\cdot\frac{1}{\omega^2}d\omega \quad (21)$$

while the total (instantaneous) noise power at the output of the integrator equals

$$P_N(t) = \frac{1}{2\pi}\int_{\omega_1}^{\omega_2}\left\{\frac{S_{\varepsilon_1}(t)}{\omega^2} + S_{\varepsilon_2}(t)\cdot\frac{E_x[G_1^2(x,t)]}{\omega^2} + S_{\varepsilon_3}(t)\cdot\frac{E_x[G_2^2(x,t)]}{\omega^2} + S_{\varepsilon_4}(t)\right\}d\omega \quad (22)$$

Hence, the average signal power at the output of the integrator equals

$$P_S = \lim_{T\to\infty}\frac{1}{T}\int_{-T/2}^{T/2} P_S(t)dt \quad (23)$$

while the total average noise power at the output of the integrator equals

$$P_N = \lim_{T\to\infty}\frac{1}{T}\int_{-T/2}^{T/2} P_N(t)dt \quad (24)$$

The dynamic range of a circuit is defined as the ratio of the maximal and the minimal signal it can handle at the same time. The maximal signal that can be handled is usually determined by signal-dependent systematic errors that arise from non-linear distortion, such as weak distortion and clipping distortion. The minimal signal that can be handled is determined by the noise with which the signal is contaminated. The dynamic range of a circuit, therefore, corresponds to the maximal signal-to-noise ratio at the output of this circuit.

Note the difference between this definition of dynamic range and another commonly used definition of dynamic range, which equals the ratio of the maximal signal a circuit can handle and the noise the circuit produces when there is no signal applied. In the linear domain, i.e. when all transfer functions are linear and the noise sources are stationary, both definitions produce the same result. In the translinear domain, however, both definitions may result in considerably different values. For this reason we adopt the term ''virtual dynamic range'' for the latter definition. Often, the virtual dynamic range is larger than the actual dynamic range.

From (23) and (24) it follows for the signal-to-noise ratio at the output of the integrator:

$$\text{SNR} = \frac{P_S}{P_N} = \frac{\lim_{T\to\infty}\frac{1}{T}P_S(t)dt}{\lim_{T\to\infty}\frac{1}{T}\int_{-T/2}^{T/2}P_N(t)dt} \quad (25)$$

Hence, we can draw the following conclusions: in order to maximize the dynamic range of the complete integrator,

- P_S must be maximal,
- $\lim_{T\to\infty}\frac{1}{T}\int_{-T/2}^{T/2} S_{\varepsilon_n}(t)dt$ must be minimal, and
- $\lim_{T\to\infty}\frac{1}{T}\int_{-T/2}^{T/2}\{S_{\varepsilon_2}(t)\cdot E_x[G_1^2(x,t)] + S_{\varepsilon_3}(t)\cdot E_x[G_2^2(x,t)]\}dt$ must be minimal.

In practice, the average noise power of the various

noise sources can be minimized by choosing current to be the information-carrying quantity insofar as possible and by operating the various subcircuits in class AB [17]. Class-AB operation also extends the dynamic range at the upper side for a given average power consumption.

Further, using

$$G_2^2(x,t) = \frac{x^2(t)}{G_1^2(x,t)} \tag{26}$$

the latter condition can be written as:

$$\lim_{T\to\infty} \frac{1}{T} \int_{-T/2}^{T/2} \left\{ S_{\varepsilon_2}(t) \cdot E_x[G_1^2(x,t)] + S_{\varepsilon_3}(t) \cdot E_x\left[\frac{x^2(t)}{G_1^2(x,t)}\right] \right\} dt \tag{27}$$

must be minimal.

As $G_1(x,t)$ appears in the numerator as well as in the denominator of (27), for each input signal x an optimal $G_1(x,t)$ and thus an optimal expanding function F can be found. Using a capacitor as a linear time integrator and the (static) translinear principle to implement the divider function, x, dy/dv, dv/dt and y become currents and, hence, F becomes an expanding transconductor. To the authors' knowledge no (static) transfer functions that are applicable have been reported other than:

- an exponential transconductor,
- a hyperbolic-sine transconductor,
- a quadratic transconductor, or
- a linear transconductor.

These transconductors and their impact on the dynamic range of the translinear integrator are discussed in the next paragraphs.

Note that the use of a linear transconductor results in a translinear integrator that is also internally linear and, therefore, not companding. In this case the translinear integrator simplifies to the well-known $g_m - C$ integrator. It is included here merely to serve as a reference.

Also note that another popular transconductor, namely the bipolar differential pair is not suited for our purposes, since it implements a tanh function, which is also not expanding. Yet, it has been suggested in [20].

The exponential transconductor. One candidate for the expanding transconductor is the exponential transfer function of a single (or compound) bipolar transistor or MOS transistor in weak inversion:

$$F(v) = I_{\text{ref}} \exp(v/V_{\text{ref}}) \tag{28}$$

I_{ref} and V_{ref} both being constants. See Fig. 3a. Since its derivative with respect to v is easily implemented ($dF/dv = F(v)/V_{\text{ref}}$), this function is at the base of most of the bipolar or weak-inversion class-A (log-domain) translinear filters.

Now suppose: $x(t) = A\omega_0 \cos(\omega_0 t)$, a sinusoidal with amplitude $A\omega_0$ and frequency ω_0. Since $y(t) = \int^t x(\tau)d\tau$ and *y(t)* must be unipolar (class-A), *y(t)* can be written as: $y(t) = A[\alpha + \sin(\omega_0 t)]$, with $\alpha > 1$. If we further, in order to come to a qualitative comparison, assume that $S_{\varepsilon_2}(t)$ and $S_{\varepsilon_3}(t)$ are constants, denoted by S_{ε_2} and S_{ε_3}, then the average noise power density spectrum resulting from ε_2 and ε_3, (27), reduces to:

$$S_{\varepsilon_2} \cdot E_x[G_1^2(x,t)] + S_{\varepsilon_3} \cdot E_x\left[\frac{x^2}{G_1^2(x,t)}\right] \tag{29}$$

which equals

$$S_{\varepsilon_2} \cdot \frac{\omega_0}{2\pi} \int_{-\pi/\omega_0}^{\pi/\omega_0} G_1^2(x,t)dt + S_{\varepsilon_3} \cdot \frac{\omega_0}{2\pi} \int_{-\pi/\omega_0}^{\pi/\omega_0} \frac{x^2}{G_1^2(x,t)} dt \tag{30}$$

which, in turn, simplifies to:

$$S_{\varepsilon_2} \cdot \frac{A^2(2\alpha^2+1)}{2V_{\text{ref}}^2} + S_{\varepsilon_3} \cdot V_{\text{ref}}^2 \omega_0^2 \frac{\alpha - \sqrt{\alpha^2-1}}{\sqrt{\alpha^2-1}} \tag{31}$$

$$= S_{\varepsilon_2} \cdot \frac{\gamma_{\text{exp}}}{V_{\text{ref}}^2} + S_{\varepsilon_3} \cdot V_{\text{ref}}^2 \omega_0^2 \delta_{\text{exp}} \tag{32}$$

γ and δ are the ''noise-multiplication factors'' and will also be derived for the other three transconductors to compare the noise performance of the four translinear integrators with each other.

The hyperbolic-sine transconductor. Another candidate for the expanding transconductor is the hyperbolic-sine transfer function of a bipolar or weak-inversion four-transistor translinear class-AB output stage:

$$\begin{aligned} F(v) &= 2I_{\text{ref}} \sinh(v/V_{\text{ref}}) \\ &= I_{\text{ref}}[\exp(v/V_{\text{ref}}) - \exp(-v/V_{\text{ref}})] \end{aligned} \tag{33}$$

See Fig. 3b. Its derivative with respect to v is also easily implemented:

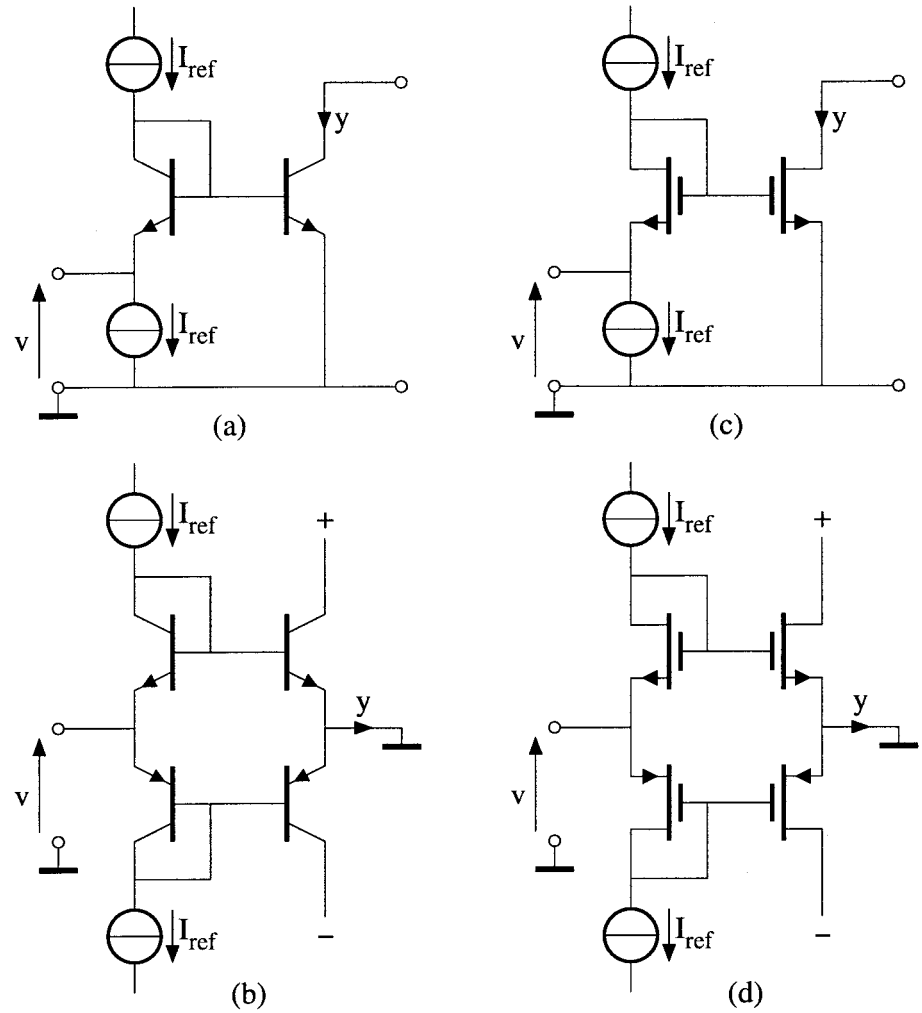

Fig. 3. Four transconductors comprising only transistors.

$$dF/dv = 2\frac{I_{\text{ref}}}{V_{\text{ref}}}\cosh(v/V_{\text{ref}}) = \frac{I_{\text{ref}}}{V_{\text{ref}}}[\exp(v/V_{\text{ref}}) + \exp(-v/V_{\text{ref}})] \quad (34)$$

The hyperbolic-sine function is at the base of most of the bipolar or weak-inversion class-AB translinear filters.

Following the same procedure as above, only now with a bipolar (class-AB) output signal $y(t) = A\sin(\omega_0 t)$, the average noise power density spectrum resulting from ε_2 and ε_3, (27), becomes

$$S_{\varepsilon_2} \cdot \frac{A^2 + 8I_{\text{ref}}^2}{2V_{\text{ref}}^2} + S_{\varepsilon_3} \cdot V_{\text{ref}}^2\omega_0^2\frac{\sqrt{A^2 + 4I_{\text{ref}}^2} - 2I_{\text{ref}}}{2I_{\text{ref}}} \quad (35)$$

$$= S_{\varepsilon_2} \cdot \frac{\gamma_{\sinh}}{V_{\text{ref}}^2} + S_{\varepsilon_3} \cdot V_{\text{ref}}^2\omega_0^2\delta_{\sinh} \quad (36)$$

The quadratic transconductor. Using MOS transistors operating in their strong inversion region, a possible expanding transconductor is the quadratic transfer function of a single or compound transistor:

$$F(v) = I_{\text{ref}}(1 + v/V_{\text{ref}})^2 \quad (37)$$

for $v > -V_{\text{ref}}$. See Fig. 3c. Its derivative with respect to v is also easily implemented:

$$dF/dv = 2\frac{I_{\text{ref}}}{V_{\text{ref}}}(1 + v/V_{\text{ref}}) \tag{38}$$

The quadratic function is at the base of the class-A $\sqrt{\ }$-domain integrators described in [12,21].

Following the same procedure as for the exponential transconductor, the average noise power density spectrum resulting from ε_2 and ε_3, (27), becomes

$$S_{\varepsilon_2} \cdot \frac{4A\alpha I_{\text{ref}}}{V_{\text{ref}}^2} + S_{\varepsilon_3} \cdot V_{\text{ref}}^2 \omega_0^2 \frac{A\left(\alpha - \sqrt{\alpha^2 - 1}\right)}{4I_{\text{ref}}} \tag{39}$$

$$= S_{\varepsilon_2} \cdot \frac{\gamma_{\text{quad}}}{V_{\text{ref}}^2} + S_{\varepsilon_3} \cdot V_{\text{ref}}^2 \omega_0^2 \delta_{\text{quad}} \tag{40}$$

The linear transconductor. A linear transistor-only transconductor stems from, for example, a strong-inversion four-transistor class-AB output stage, as introduced by Bult in [22]:

$$\begin{aligned} F(v) &= I_{\text{ref}}\left((1 + v/V_{\text{ref}})^2 - (1 - v/V_{\text{ref}})^2\right) \\ &= 4I_{\text{ref}} v/V_{\text{ref}} \end{aligned} \tag{41}$$

See Fig. 3d. Its derivative with respect to v equals $4I_{\text{ref}}/V_{\text{ref}}$, a constant.

Following the same procedure as for the hyperbolic-sine transconductor, the average noise power density spectrum resulting from ε_2 and ε_3, (27), becomes

$$S_{\varepsilon_2} \cdot \frac{16I_{\text{ref}}^2}{V_{\text{ref}}^2} + S_{\varepsilon_3} \cdot V_{\text{ref}}^2 \omega_0^2 \frac{A^2}{32I_{\text{ref}}^2} \tag{42}$$

$$= S_{\varepsilon_2} \cdot \frac{\gamma_{\text{lin}}}{V_{\text{ref}}^2} + S_{\varepsilon_3} \cdot V_{\text{ref}}^2 \omega_0^2 \delta_{\text{lin}} \tag{43}$$

A comparison. Now that the influence of the various noise sources on the integrator's output signal is known—ε_1 and ε_4 are simply added to x and y, respectively, and, therefore, their noise contributions are not influenced by the transconductor choice—, the four transconductors can be compared with respect to their influence on the average noise power density spectrum resulting from ε_2 and ε_3, according to (31), (35), (39) and (42).

Table 1 summarizes the various noise multiplication factors γ and δ.

Straightforward calculations on these noise multiplication factors reveal that, for every arbitrary sinusoidal input signal and noise sources ε_2 and ε_3 being equal for all four integrators:

- for all transconductors, the output noise increases with an increasing signal amplitude A. This corresponds to the results obtained in [11,23–25];
- the hyperbolic-sine transconductor, the quadratic transconductor and the linear transconductor can be optimized by means of a proper reference current I_{ref},
- the exponential transconductor can be optimized by means of a proper choice of α,
- an optimized hyperbolic-sine transconductor yields a lower noise contribution than an optimized exponential transconductor,
- an optimized linear transconductor yields a lower noise contribution than an optimized quadratic transconductor and
- an optimized linear transconductor yields a lower noise contribution than an optimized hyperbolic sine transconductor.

Taking into account that the noise powers of $\varepsilon_2(t)$ and $\varepsilon_3(t)$ can be smaller when the circuit is operated in class AB than when the circuit is operated in class A and that for a given signal current the thermal noise generated by a MOS transistor in strong inversion will be smaller than the shot noise of a bipolar transistor or weak-inversion MOS transistor, it becomes clear that indeed the lowest noise contribution is achieved with the four-transistor strong-inversion transconductor.

However, comparing the four integrators at the upper side of the dynamic range, thus the transconductor's output capability:

- the output signal amplitude of the exponential transconductor is limited to I_{ref},

Table 1. Comparison of the various noise multiplication factors γ and δ.

Transconductor	γ	δ
$F(v) = I_{\text{ref}} \exp(v/V_{\text{ref}})$	$\frac{A^2(2\alpha^2+1)}{2}$	$\frac{\alpha-\sqrt{\alpha^2-1}}{\sqrt{\alpha^2-1}}$
$F(v) = 2I_{\text{ref}} \sinh(v/V_{\text{ref}})$	$\frac{A^2+8I_{\text{ref}}^2}{2}$	$\frac{\sqrt{A^2+4I_{\text{ref}}^2}-2I_{\text{ref}}}{2I_{\text{ref}}}$
$F(v) = I_{\text{ref}}(1 + v/V_{\text{ref}})^2$	$4A\alpha I_{\text{ref}}$	$\frac{A(\alpha-\sqrt{\alpha^2-1})}{4I_{\text{ref}}}$
$F(v) = 4I_{\text{ref}} v/V_{\text{ref}}$	$16I_{\text{ref}}^2$	$\frac{A^2}{32I_{\text{ref}}^2}$

- the output signal amplitude of the hyperbolic-sine transconductor is unlimited,
- the output signal amplitude of the quadratic transconductor is limited to I_{ref} and
- the output signal amplitude of the linear transconductor is limited by V_{ref} and thus to $4I_{\text{ref}}$.

From the above observations two important conclusions can be drawn:

- **if, for a given range of input signals, the signal voltage swing inside the integrator is not limited by the circuit or its power supply, the strong-inversion class-AB translinear integrator has the largest dynamic range, and**
- **if, for a given range of input signals, the voltage swing inside the integrator is limited by the circuit and/or its power supply, the class-AB hyperbolic-sine integrator has the largest dynamic range.**

Of course, in practice, the dynamic range of the hyperbolic-sine integrator will be limited by various transistor second-order effects, such as base currents, series resistances, high-level injection and finite transit frequencies. However, many of these effects can be counteracted by careful circuit and layout design.

From the above observations it also follows that there are no reasons to choose for an exponential or quadratic transconductor from a dynamic-range point of view. Only in ultra-low-power applications, where resistors would become too large for integration, and all active devices behave exponentially, dynamic translinear techniques may be the only way to implement inherently linear continuous-time transfer functions [13]. The quadratic transconductor, as found in $\sqrt{\ }$-domain integrators may be interesting from an academic point of view, but does not seem to have any practical value.

4. Design Example

In the previous section, it was shown that the hyperbolic-sine integrator is a promising circuit for high-dynamic-range signal processing, even at low supply voltages, and that its noise contribution can be minimized by choosing a proper bias current I_{ref}. For this reason, a $\pm$ 1.65-V bipolar class-AB translinear integrator has been designed, using standard translinear techniques. Its circuit diagram is depicted in Fig. 4.

Both the sinh and cosh functions are implemented by the translinear loop comprising transistors Q_1 through Q_4. The difference between the collector currents of Q_2 and Q_3 equals the integrator output signal $I_{\text{sinh}} = 2I_Z \sinh(v/V_T) = F(v)$, V_T being the thermal voltage kT/q. The sum of these collector currents equals $I_{\text{cosh}} = 2I_Z \cosh(v/V_T) = V_T dF(v)/dv$. Note the difference in dimension

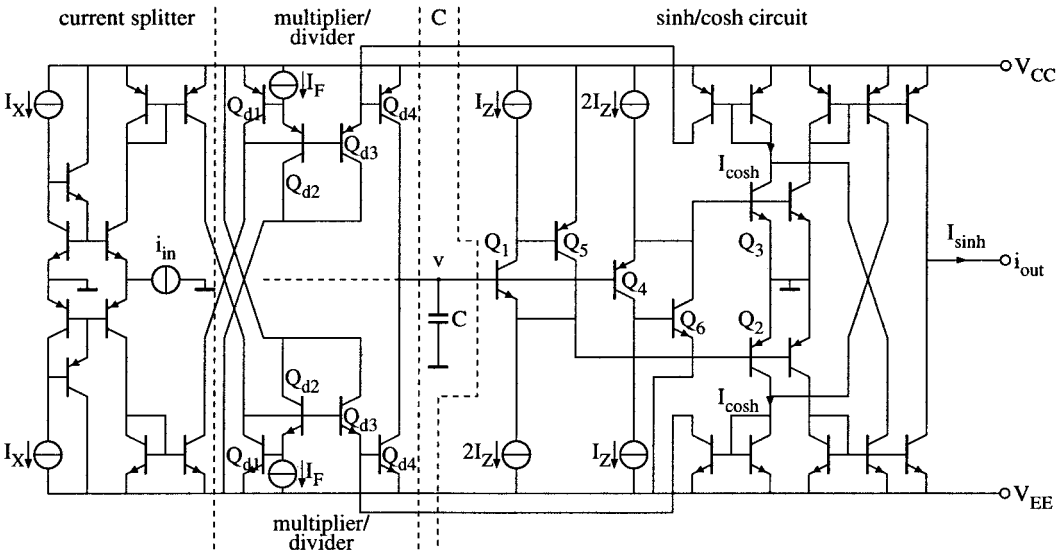

Fig. 4. Circuit diagram of the bipolar class-AB translinear integrator.

between $I_{\cosh}$ and $dF(v)/dv$ in Fig. 1, which originates from the term V_T.

Current I_Z can be used to optimize the dynamic range of the complete integrator according to (27) with the aid of a circuit simulator. Note that, apart from $G_1(x,t)$ and $G_2(x,t)$, also the noise power-density spectra $S_{\varepsilon_2}(t)$ and $S_{\varepsilon_3(t)}$ depend on the momentary signal values, which, in turn, depend on the integrator input signal and the implemented class-AB behavior. For this reason, a mathematical expression for the optimal value of I_Z is not easily found.

To increase the input impedance, which is directly related to the integrator DC gain, two common-emitter stages, Q_5 and Q_6, have been added.

The class-AB divider is implemented by two class-A ''log-antilog'' multiplier/dividers [18] (Q_{d1} through Q_{d4}), each processing one half of the signal. I_F is a normalizing constant, for the output of the translinear multiplier/divider is also a current. Since the operation of a single multiplier/divider is limited to one quadrant only and because I_F and $I_{\cosh}$ are already unipolar, the integrator input signal is split into two unipolar currents that can be processed separately. This is done by the class-AB push-pull stage at left. The output currents of this current splitter equal

$$\frac{\pm i_{\text{in}} + \sqrt{i_{\text{in}}^2 + 4I_X^2}}{2}.$$

Current source I_X determines the class-AB behavior of the splitter and thus of the complete integrator. To make the flow of output currents larger than βI_X possible (β being the (signal- and frequency-dependent!) large-signal current gain factor of a transistor), two additional (non-inverting) amplifiers that supply the base currents of these four transistors have been added. After the multiplication/division, both signals are added in capacitor C in order to restore the original bipolarity.

The transfer function of this translinear integrator equals: $I_{\sinh} = \frac{I_F}{V_T C}\int i_{\text{in}} dt$. It can be seen that the integrator time constant τ $(= V_T C/I_F)$ can easily be controlled over a wide range by means of I_F. Note

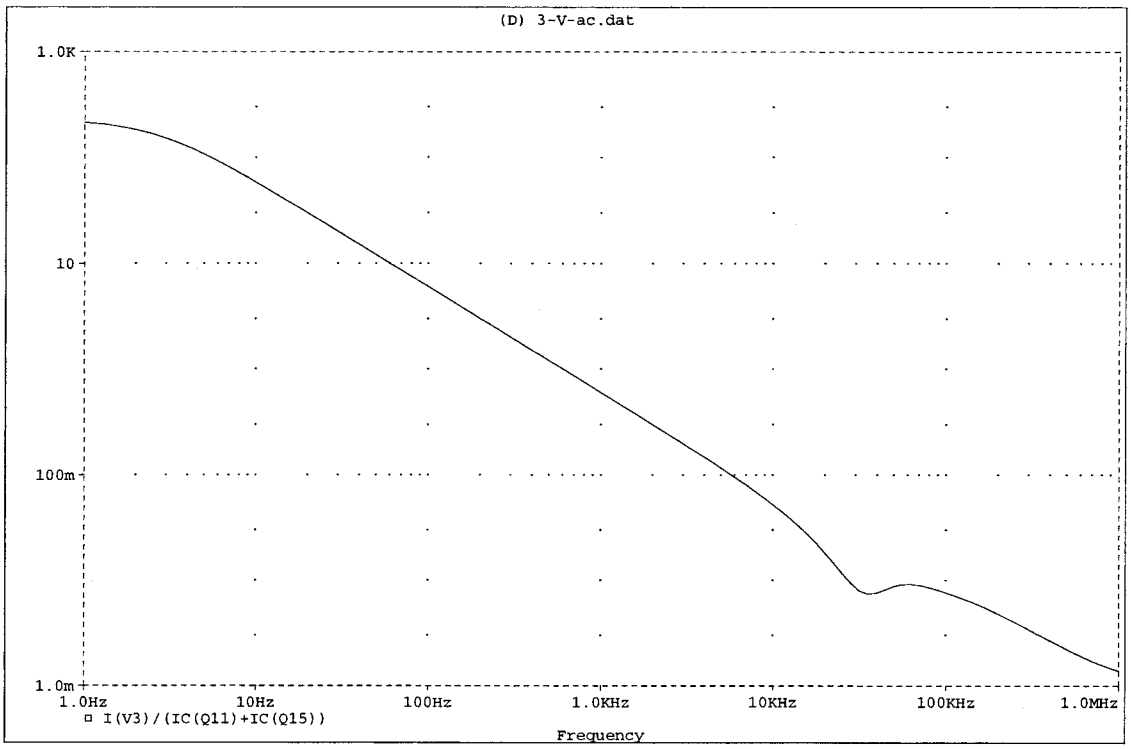

Fig. 5. Simulated small-signal frequency response of the bipolar class-AB translinear integrator for $I_X = I_F = I_Z = 10$ nA and $C = 100$ pF.

that, if I_F is made proportional to the absolute temperature (PTAT), τ becomes independent of the temperature [5,6].

Experimental results. The circuit shown in Fig. 4 was simulated using SPICE and realistic (IC) capacitor and (minimum-size) transistor models, extracted from our in-house 2-μm, 7-GHz bipolar IC process. Typical transistor parameters are: $h_{\mathrm{fe,NPN}} \approx 100$, $f_{\mathrm{T,NPN}} \approx 7$ GHz, $h_{\mathrm{fe,LPNP}} \approx 80$ and $f_{\mathrm{T,LPNP}} \approx 40$ MHz. The results indicate the correct operation of the translinear integrator for various temperatures and values of I_F, I_X, I_Z and C.

Fig. 5 shows the simulated small-signal frequency response for $I_X = I_F = I_Z = 10$ nA and $C = 100$ pF at 273 K. The unity-gain frequency equals 610 Hz. It can be seen that the integrator bandwidth, i.e. the frequency range over which the integrator transfer deviates less than 3 dB from the ideal transfer of 20 dB per decade, is limited, at low frequencies by the finite DC gain, which, in turn, results from the limited current gain factor of the transistors in the rightmost current mirrors and, at high frequencies, by the limited transit frequency of the transistors resulting from the low collector bias currents.

Fig. 6 depicts the simulated transient response for a 10 nA (peak value), 1 kHz; input signal, for the same control currents as above. Thus the peak value of the input signal equals the quiescent current I_X. The upper curve shows the integrator output signal analyzed in the frequency domain, while the lower curve shows the same signal in the time domain. The total harmonic distortion in this situation equals 0.12%.

Fig. 7 also depicts the integrator output signal, but now for a 100 nA (peak value) input signal, which equals ten times the quiescent current I_X. In this situation, the total harmonic distortion equals 2.0%.

Fig. 8 again shows the integrator output signal, but now for a 1 μA (peak value) input signal, thus hundred times I_X. Clearly, the effects of the limited transistor current gain factors are visible: both the peaks and the zero-crossings become severely distorted. These effects are known as soft clipping and cross-over distortion. Due to these distortion

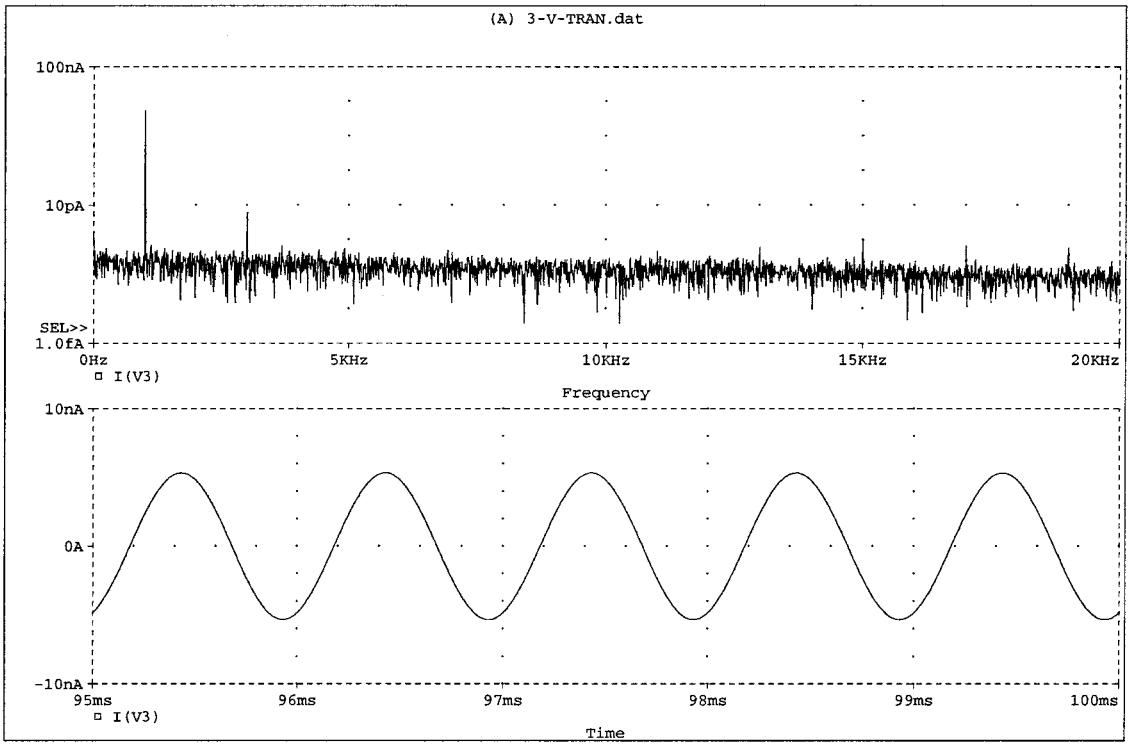

Fig. 6. Simulated transient response for a 10 nA (peak value), 1 kHz; input signal, in the frequency domain (upper curve) and in the time domain (lower curve). The total harmonic distortion equals 0.12%.

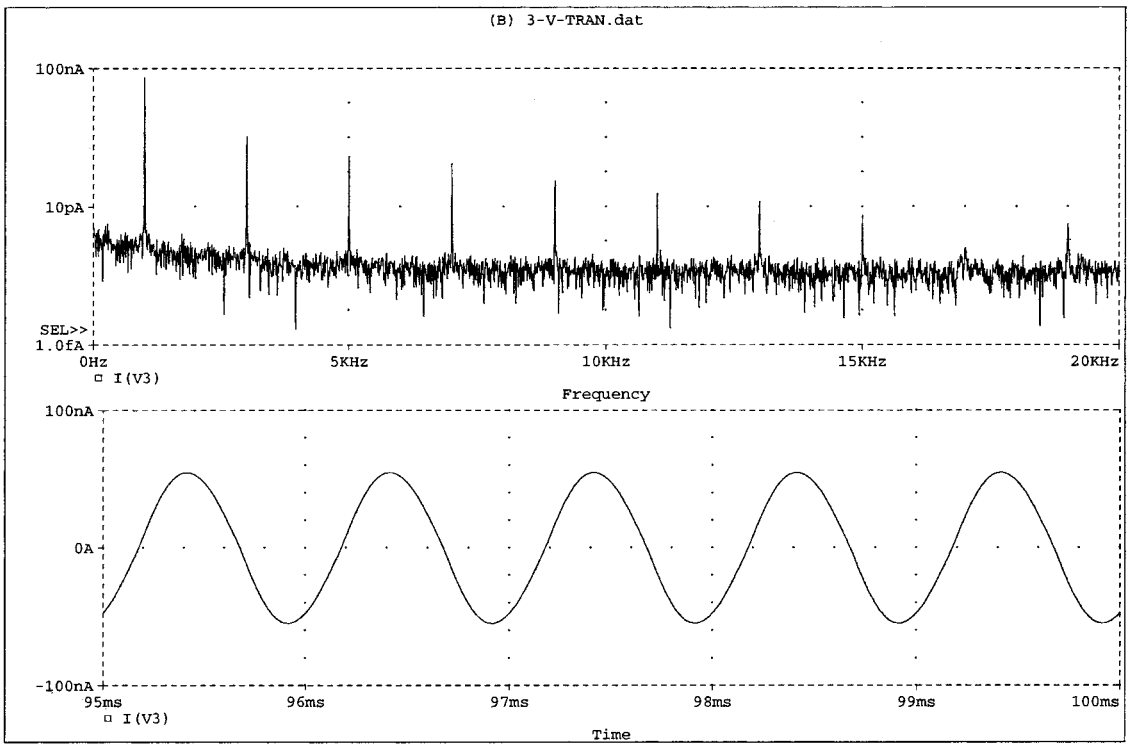

Fig. 7. Simulated transient response for a 100 nA (peak value), 1 kHz; input signal, in the frequency domain (upper curve) and in the time domain (lower curve). The total harmonic distortion equals 2.0%.

mechanisms, the total harmonic distortion equals 10%.

Fig. 9 indicates the influence of a stationary noise source, located at the output of the multiplier/divider, thus corresponding with ε_2 in the previous noise analysis. The pseudo-random noise signal, shown in the uppermost curve, comprises 12 sinusoidal signals and is characterized by a noise bandwidth from 100 Hz to 10 kHz; and an average noise power of 14 aA^2. This value is much larger than the noise of the given circuit and its bias and signal currents, but demonstrates exactly what happens for changes in the noise-optimization current I_Z. The lower three curves show the integrator output current for I_Z equal to 3.2 nA, 10 nA and 32 nA, respectively. It can be seen that the resulting noise at the output becomes smaller for smaller values of I_Z, thus for smaller values of $E_x[G_1^2(x,t)]$, in correspondence with (27). Also note that the noise mainly affects the peaks of the sinusoid, thus for large values of $dF(v(t))/dv(t)$. This is in line with (10) and (20).

The influence of a stationary noise source ε_3 is depicted in Fig. 10. The same pseudo-random noise signal is used, but now inserted at the output of the block $dF(v)/dv$. Now, the resulting noise at the output becomes smaller for larger values of I_Z, thus for smaller values of $E_x[G_2^2(x,t)]$, in correspondence with (27). Also note that the noise mainly affects the zero-crossings of the sinusoid, thus for small values of $dF(v(t))/dv(t)$. This is in line with (11) and (20). From Figs. 9 and 10, it will be clear that, when ε_2 and ε_3 are in the same order of magnitude, which is the case for the underlying translinear integrator, an optimum I_Z can be found. In this situation, this optimum lies around 12 nA.

To verify the circuit operation in practice, the class-AB translinear integrator was implemented in a bread-board realization, using transistor arrays, fabricated in a standard 2.5 μm BiCMOS IC process. Fig. 11 shows a photograph of the breadboard circuit. For biasing purposes, the integrator was enclosed in a unity-feedback configuration, which results in a first-order low-pass filter with a cutoff frequency of $\frac{I_F}{2\pi V_T C}$ Hz.

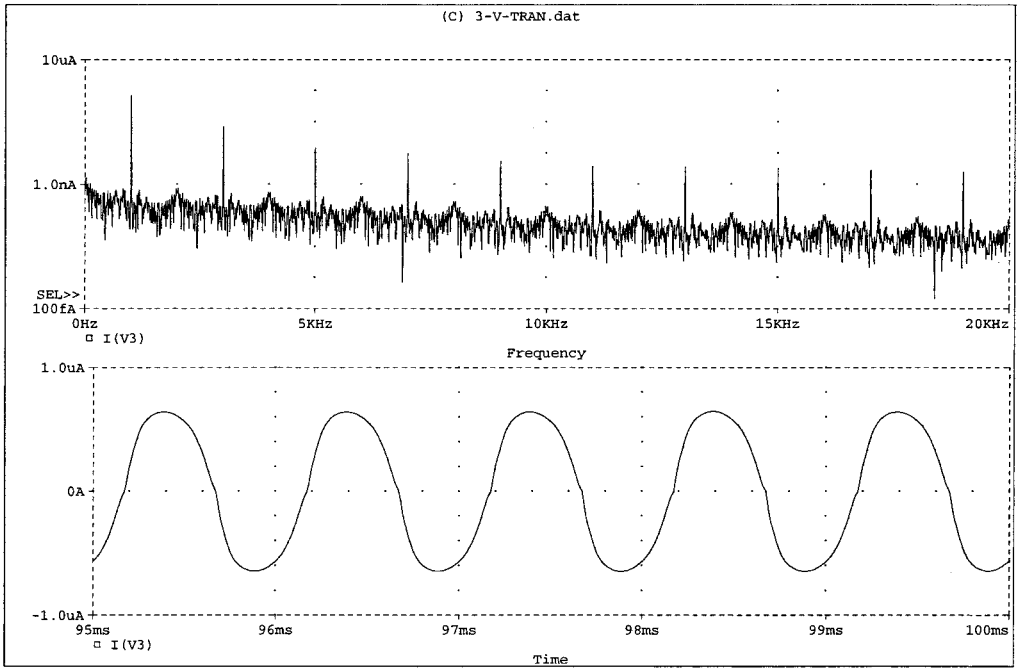

Fig. 8. Simulated transient response for a 1 μA (peak value), 1 kHz; input signal, in the frequency domain (upper curve) and in the time domain (lower curve). The total harmonic distortion equals 10%.

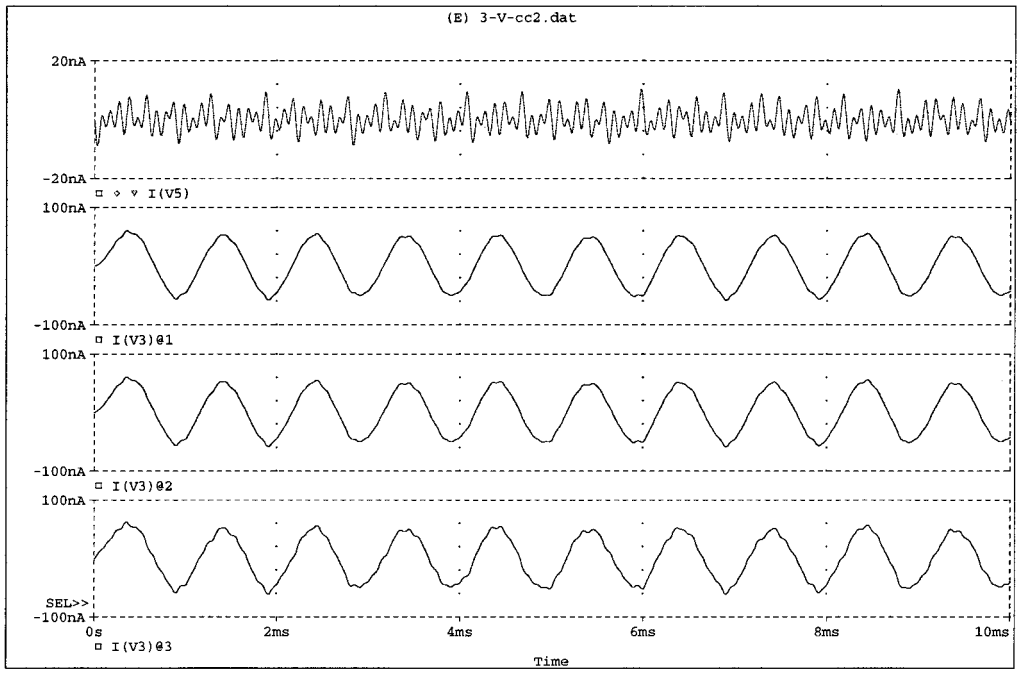

Fig. 9. Simulated transient response of the integrator in unity-feedback configuration for a 100 nA (peak value), 1 kHz input signal and a pseudo-random noise signal ε_2, characterized by a noise bandwidth from 100 Hz to 10 kHz; and an average noise power of 14 aA^2, for three different values of the noise-optimization current I_Z. The uppermost curve shows the pseudo-random noise signal. The lower curves show the output current for I_Z equal to 3.2 nA, 10 nA and 32 nA, respectively.

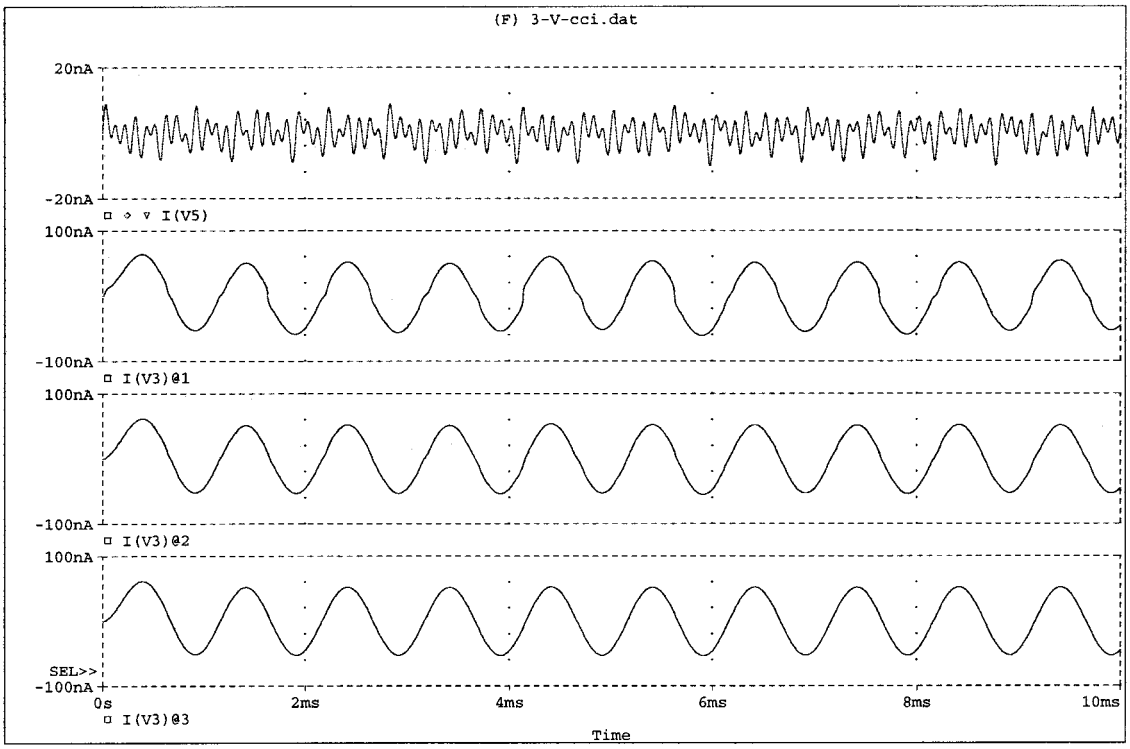

Fig. 10. Simulated transient response of the integrator in unity-feedback configuration for a 100 nA (peak value), 1 kHz input signal and a pseudo-random noise signal ε_3, characterized by a noise bandwidth from 100 Hz to 10 kHz; and an average noise power of 14 aA^2, for three different values of the noise-optimization current I_Z. The uppermost curve shows the pseudo-random noise signal. The lower curves show the output current for I_Z equal to 3.2 nA, 10 nA and 32 nA, respectively.

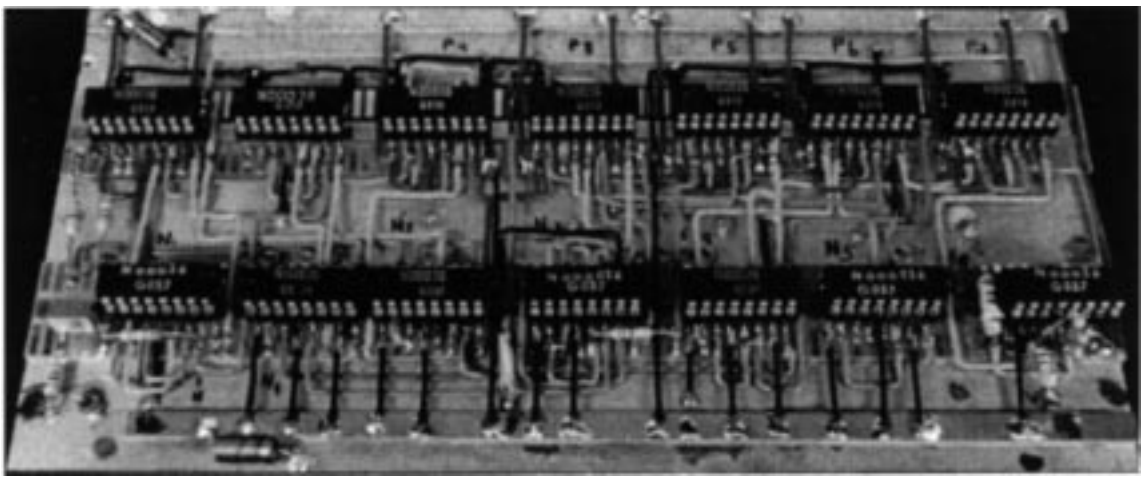

Fig. 11. Bread-board realization of the class-AB translinear integrator.

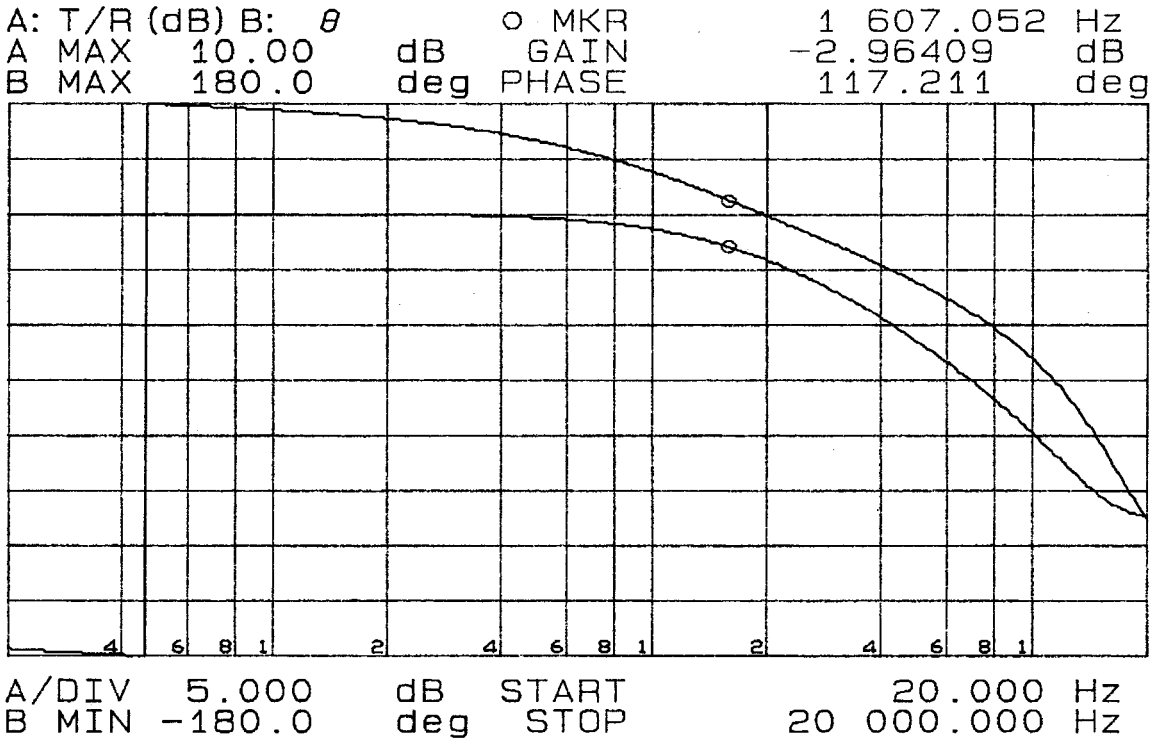

Fig. 12. Measured frequency response of the integrator in unity-feedback configuration for a 100 nA (peak value) input signal.

Subsequently, the circuit was optimized for audio signals in a frequency range from 100 Hz to 10 kHz; and a cutoff frequency of 1.6 kHz;. For $C = 100$ pF and $T = 293$ K (room temperature), I_F must equal 26 nA. Current I_X sets the high-frequency behavior of the filter and was chosen to be equal to 10 nA in order to cope with the large parasitic capacitances of the bread-board realization. The measured frequency response hardly depended on I_Z, as expected. Fig. 12 shows the measured frequency response (both magnitude and phase) of the integrator in unity-feedback configuration for a 100 nA (RMS) input signal. The effect of the low transistor transit frequencies, resulting from the relatively small value of I_X is clearly visible.

The actual choice of I_Z was based on similar simulations as described above. 13 nA turned out to be a convenient value for a 100 nA (RMS), 1-kHz sinusoid input signal. Fig. 13 shows the measured transient response of the integrator in unity-feedback configuration for three different magnitudes of the input signal, being zero, 100 nA (RMS) and 400 nA (RMS), respectively. In the latter situation, the total harmonic distortion equals 2%. Together with the measured noise of 280 pA (RMS), this yields a dynamic range, i.e. a maximal signal-to-noise ratio, of 63 dB. Also the influence of the signal magnitude on the total output noise, i.e. the signal × noise intermodulation, is clearly visible: for larger input currents the output noise also becomes larger, which is in correspondence with equation (35). The virtual dynamic range, thus the ratio of the maximal signal the integrator can handle and the noise that is produced when there is no signal applied, equals 76 dB. The supply voltage and the quiescent current equal 3.3 V ($\pm$ 1.65 V) and 310 nA, respectively.

5. Conclusions

In this paper we derived several design principles to achieve an optimal dynamic range in translinear

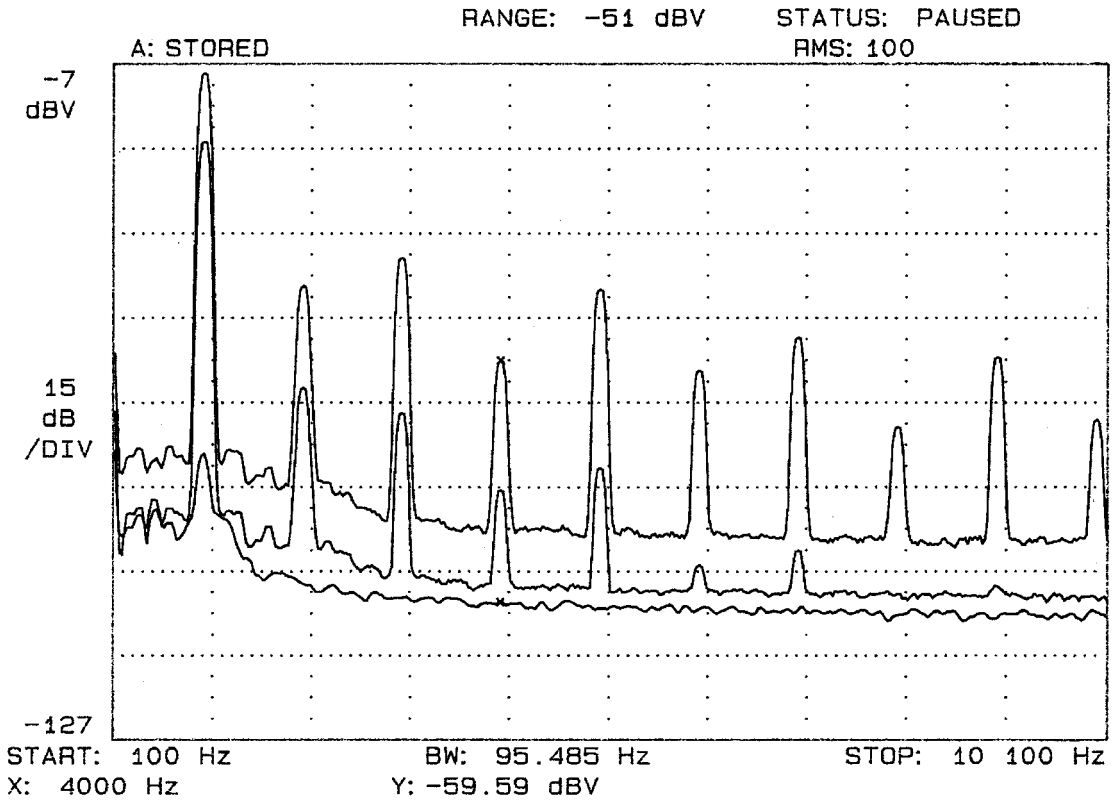

Fig. 13. Measured transient response of the integrator in unity-feedback configuration.

integrators. It turned out that, for four representative integrator structures,

- if, for a given range of input signals, the signal voltage swing inside the integrator is not limited by the circuit or its power supply, the class-AB translinear integrator, employing MOS transistors operating in their strong-inversion region, has the largest dynamic range, and
- if, for a given range of input signals, the voltage swing inside the integrator is limited by the circuit and/or its power supply, the class-AB translinear integrator, employing bipolar transistors or MOS transistors operating in their weak-inversion region, has the largest dynamic range.

As an example, a $\pm$ 1.65 V translinear integrator was presented that makes dynamic-range optimization possible by adjusting just one bias current. Its application in an audio filter yields a 63-dB dynamic range and a virtual dynamic range of 76 dB, while the current consumption can be as low as 310 nA.

Acknowledgments

The authors would like to thank Rob van Beijnhem for the bread-board realization of the test circuit. This research was funded by the Dutch Technology Foundation (STW), project DEL33.3251.

References

1. J. Mulder, A. C. van der Woerd, W. A. Serdijn, and A. H. M. van Roermund, ''General current-mode analysis of translinear filters.'' *IEEE Transactions on Circuits and Systems* 44(3), pp. 193–197, 1997.

2. J. Mulder, W. A. Serdijn, A. C. van der Woerd, and A. H. M. van Roermund, ''Analysis and synthesis of dynamic translinear circuits.'' *proc. ECCTD'97* Budapest, 1, pp. 18–23, 1997.
3. A. C. van der Woerd, J. Mulder, W. A. Serdijn, and A. H. M. van Roermund, ''Recent trends in translinear integrated circuits.'' *proc. Electronics—ET'96* Sozopol, Bulgaria, 1996.
4. B. Gilbert, ''Translinear circuits: a proposed classification.'' *Electronics Letters* 11(1), pp. 14–16, 1975.
5. R. W. Adams, ''Filtering in the log domain.'' Preprint No. 1470, presented at the 63rd AES Conference, New York, 1979.
6. E. Seevinck, ''Companding current-mode integrator: a new circuit principle for continuous-time monolithic filters.'' *Electronics Letters* 26(24), pp. 2046–2047, 1990.
7. D. R. Frey, ''Log-domain filtering: an approach to current-mode filtering.'' *IEE Proc. Pt. G* 140(6), pp. 406–416, 1993.
8. M. Punzenberger and C. C. Enz, ''Low-voltage companding current-mode integrators.'' *Proc. IEEE ISCAS* Seattle, pp. 2112–2215, 1995.
9. C. Toumazou, J. Ngarmnil, and T. S. Lande, ''Micropower log-domain filter for electronic cochlea.'' *Electronics Letters* 30(22), pp. 1839–1841, 1994.
10. D. Perry and G. W. Roberts, ''Log-domain filters based on LC ladder synthesis.'' *Proc. IEEE ISCAS* Seattle, pp. 311–314, 1995.
11. Y. Tsividis, ''Externally linear, time-invariant systems and their application to companding signal processors.'' *IEEE Transactions on Circuits and Systems-II* 44(2), pp. 65–85, 1997.
12. J. Mulder, A. C. van der Woerd, W. A. Serdijn, and A. H. M. van Roermund, ''A current-mode companding $\sqrt{x}$-domain integrator.'' *Electronics Letters* 32(3), pp. 198–199, 1996.
13. W. A. Serdijn, M. Broest, J. Mulder, A. C. van der Woerd, and A. H. M. van Roermund, ''A low-voltage ultra-low-power translinear integrator for audio filter applications.'' *IEEE Journal of Solid-State Circuits* 32(4), pp. 577–581, 1997.
14. J. Mulder, A. C. van der Woerd, W. A. Serdijn, and A. H. M. van Roermund, ''An RMS-DC converter based on the dynamic translinear principle.'' *IEEE Journal of Solid-State Circuits* 32(7), 1997.
15. W. A. Serdijn, J. Mulder, A. C. van der Woerd, and A. H. M. van Roermund, ''The design of wide-tunable translinear second-order oscillators.'' *proc. IEEE ISCAS'97* Hong Kong, 2, pp. 829–832, 1997.
16. W. A. Serdijn, A. C. van der Woerd and A. H. M. van Roermund, ''Chain-rule resistance: a new circuit principle for inherently linear ultra-low-power on-chip transconductances or transresistances.'' *Electronics Letters* 32(4), pp. 277–278, 1996.
17. W. A. Serdijn, A. C. van der Woerd, A. H. M. van Roermund, and J. Davidse, ''Design principles for low-voltage low-power analog integrated circuits.'' *Analog Integrated Circuits and Signal Processing* 8, pp. 115–120, 1995.
18. B. Gilbert, ''Current-mode circuits from a translinear viewpoint: a tutorial.'' in: C. Toumazou, F. J. Lidgey and D. G. Haigh (editors): *Analogue IC design: the current-mode approach*. Peter Peregrinus, London, 1990.
19. D. G. Lampard, ''Generalization of the Wiener-Khintchine theorem to nonstationary processes.'' *Journal of Applied Physics* 25(6), pp. 802–803, 1954.
20. D. R. Frey, ''Exponential state space filters: a generic current mode design strategy.'' *IEEE Transactions on Circuits and Systems—I* 43(1), pp. 34–42, 1996.
21. M. H. Eskiyerli, A. J. Payne, and C. Toumazou, ''State-space synthesis of integrators based on the MOSFET square law.'' *Electronics Letters* 32(3), pp. 198–199, 1996.
22. K. Bult and H. Wallinga, ''A class of analog CMOS circuits based on the square-law characteristics of an MOS transistor in saturation.'' *IEEE Journal of Solid-State Circuits* 22(6), pp. 357–365, 1987.
23. C. C. Enz, ''Low-power log-domain continuous-time filters: an introduction.'' *Low-Power Low-Voltage Workshop at ESSCIRC'95*, 1995.
24. M. Punzenberger and C. C. Enz, ''A 1.2-V BiCMOS class-AB log-domain filter.'' *Proc. ISSCC* pp. 56–57, 1997.
25. J. Mulder, M. H. L. Kouwenhoven, and A. H. M. van Roermund, ''Signal × noise intermodulation in translinear filters.'' *Electronics Letters* 33(14), pp. 1205–1207, 1997.

Wouter Serdijn was born in Zoetermeer, The Netherlands, in 1966. He started his course at the Faculty of Electrical Engineering at the Delft University of Technology in 1984, and received his 'ingenieurs' (M.Sc.) degree in 1989.

Subsequently, he joined the Electronics Research Laboratory of the same university where he received his Ph.D. in 1994. His research interests include low-voltage, ultra-low-power, RF and dynamic-translinear analog integrated circuits along with circuits for wireless communications, hearing instruments and pacemakers. Since 1997, he is a project leader in the multi-disciplinary *Ubiquitous Communications (UbiCom)* research program of the Delft University of Technology. He is co-editor and co-author of the book *Analog IC Techniques for Low-Voltage Low-Power Electronics* (Delft University Press, Delft, 1995), and of the book *Low-Voltage Low-Power Analog Integrated Circuits* (Kluwer Academic Publishers, Boston, 1995). He authored and co-authored more than 40 publications. He teaches *Analog Electronics for Industrial Designers, Analog IC Techniques* and *Electronic Design Techniques*.

Michiel Kouwenhoven was born in Delft, The Netherlands, on July 8, 1971. He received the M.Sc. degree in electrical engineering from Delft University of Technology in 1993, and the Ph.D. degree from the same University of Technology in 1993, and the Ph.D. degree from the same university in 1998. Since October 1997, he is an assistant professor at the Electronics Research Laboratory. His research interests include noise in non-linear circuits and systems, and RF communication systems.

Jan Mulder was born in Medemblik, The Netherlands on July 7, 1971. He received the M.Sc. degree in electrical engineering from the Delft University of Technology in 1994. Since 1994 he is working towards his Ph.D. thesis on static and dynamic-translinear analog integrated circuits, at the Electronics Research Laboratory.

Arthur H. M. van Roermund was born in Delft, The Netherlands in 1951. He received the M.Sc. degree in electrical engineering in 1975 from Delft University of Technology and the Ph.D. degree in Applied Sciences from the K. U. Leuven, Belgium, in 1987.

From 1975 to 1992 he was with the Philips Research Laboratories in Eindhoven. First he worked in the Consumer Electronics Group on design and integration of analog circuits and systems, especially switched-capacitor circuits. In 1987 he joined the Visual Communications Group where he has been engaged in video architectures and digital video signal processing. From 1987 to 1990 he was project leader of the Video Signal Processor project and from 1990 to 1992 of a Multi-Window Television project. Since 1992 he is a full professor at the Electrical Engineering Department of the Delft University of Technology where he is heading the Electronics Research Laboratory. He is also group leader of the Electronics Group and co-ordinator of the Circuits and Systems Section of DIMES: the Delft Institute of Micro Electronics and Submicron technology, which is a co-operation between research groups on micro electronics, technology and technology-related physics.